Mott variable-range hopping and weak antilocalization effect in heteroepitaxial Na_2IrO_3 thin films

Marcus Jenderka,* José Barzola-Quiquia, Zhipeng Zhang, Heiko Frenzel, Marius Grundmann, and Michael Lorenz
Institut für Experimentelle Physik II, Universität Leipzig, Linnéstraße 5, D-04103 Leipzig, Germany
(Received 21 March 2013; published 8 July 2013)

Iridate thin films are a prerequisite for any application utilizing their cooperative effects resulting from the interplay of strong spin-orbit coupling and electronic correlations. Here, heteroepitaxial Na_2IrO_3 thin films with (001) out-of-plane crystalline orientation and well-defined in-plane epitaxial relationship are presented on various oxide substrates. Resistivity is dominated by a three-dimensional variable-range hopping mechanism in a large temperature range between 300 K and 40 K. Optical experiments show the onset of a small optical gap $E_{go} \approx 200$ meV and a splitting of the Ir $5d$-t_{2g} manifold. Positive magnetoresistance below 3 T and 25 K shows signatures of a weak antilocalization effect.

DOI: 10.1103/PhysRevB.88.045111 PACS number(s): 68.55.−a, 71.27.+a, 75.50.Lk

Transition-metal oxides containing $5d$ iridium ions allow for the observation of novel cooperative effects resulting from an interplay between strong spin-orbit coupling and electronic correlations. These iridates are promising candidates for high-T_C superconductors,[1] spin liquids,[2–4] a novel $J_{\text{eff}} = 1/2$ Mott-insulating ground state,[5,6] and topological insulators.[7–10]

A rather recently studied iridate is the Mott-insulating layered compound Na_2IrO_3 where edge-sharing IrO_6 octahedra form a honeycomb lattice within each Na_2IrO_3 layer.[11] Theoretical studies of magnetic interactions in model Hamiltonians of A_2BO_3-type compounds[12,13] suggest spin liquid behavior in Na_2IrO_3. On the other hand, tight-binding model analyses and first-principles band structure calculations,[7,10,14] as well as density-matrix renormalization group calculations,[15] suggest Na_2IrO_3 as a possible topological insulator. Both states of matter, however, promise possible application in fault-tolerant quantum computation.[16–18]

Experimental efforts on Na_2IrO_3 were so far limited to powder and single-crystalline samples.[11,19–22] Initially, from x-ray diffraction experiments a monoclinic $C2/c$ unit cell for Na_2IrO_3 was suggested.[11] More recent experiments however are more consistent with a $C2/m$ unit cell.[19,20] Later experiments also confirm the presence of trigonal distortions of the IrO_6 octahedra and that structural disorder, i.e., stacking faults and Na/Ir site mixings, is common. The compound furthermore exhibits frustrated antiferromagnetic order below $T_N = 15$ K with moments ordered collinearly in a zigzag pattern.[19–21] Furthermore, single-crystalline Na_2IrO_3 has a small band gap.[22] Its temperature-dependent in-plane dc electrical resistivity follows a $\rho \propto \exp[(T_0/T)^{1/4}]$ behavior between 100 and 300 K.[11] Such a $\rho(T)$ dependence is usually associated with three-dimensional Mott variable range hopping[23] of localized carriers.

In this paper, we report on heteroepitaxial Na_2IrO_3 thin films grown on (001) $YAlO_3$, a-sapphire, and c-sapphire. Deposition of Na_2IrO_3 thin films ultimately is a step towards future device applications of this material. Our heteroepitaxial films exhibit a clear epitaxial relation and an excellent (001) out-of-plane orientation. In magnetoresistance measurements we observe the weak antilocalization effect at 25 K and below.

Thin films were grown by pulsed laser deposition (PLD) on 5×5 mm^2 and 10×10 mm^2 a-plane (11.0) sapphire, c-plane (001) sapphire, and $YAlO_3$ (001) single crystals at temperatures and oxygen partial pressures ranging from about 550 °C to 650 °C and from 0.6 mbar to 3.0×10^{-4} mbar, respectively. PLD was done with a 248 nm KrF excimer laser at a laser fluence of 2 J cm^{-2}. The polycrystalline Na_2IrO_3 target was prepared by a solid-state synthesis, according to Ref. 11. First ellipsometry measurements could only give a rough estimate of film thickness between 400 and 800 nm which, however, is still consistent with PLD growth rates for other oxide thin films.[24] More detailed information about target preparation and film deposition can be found in the Supplemental Material. [25]

For structural analysis we employed a Philips X'Pert x-ray diffractometer equipped with a Bragg-Brentano powder goniometer using divergent/focusing slit optics and Cu K_α radiation. Surface morphology was investigated via a Park System XE-150 atomic force microscope in dynamic non-contact mode. Temperature-dependent dc electrical resistivity was measured in van der Pauw geometry. Transverse magnetoresistance was measured with a high-resolution AC bridge (LR700 from Linear Research) in a commercial cryostat in the temperature range between 5 and 100 K with magnetic fields up to 8 T in both van der Pauw and four-point geometry with sputtered gold contacts. Optical transmission was measured at ambient conditions and room temperature within a total photon energy range from 0.025 to 6.2 eV. For the interval from 0.025 to 0.992 eV we employed a BRUKER IFS 66v/S Fourier transform infrared spectrometer (FTIR). The spectral range from 0.62 to 6.20 eV was covered by a Perkin Elmer Lambda 40 UV/VIS spectrometer. We further measured photoconductance which was obtained from the slope $1/R$ of current-voltage characteristics measured using an Agilent 4156C Precision Semiconductor Parameter Analyzer under illumination from a xenon arc lamp. The incident photon energy was tuned via a monochromator from 0.72 to 4.96 eV.

Typical x-ray diffraction (XRD) patterns of a series of Na_2IrO_3 thin films grown on $YAlO_3$ (YAO) (001) at $T \approx 550$ °C and at oxygen partial pressures p_{O2} as indicated are displayed in Fig. 1(a). The patterns are indexed according to the JCPDS diffraction database pattern 00-026-1376 for Na_2IrO_3 in the monoclinic $C2/c$ unit cell. The patterns show very pronounced symmetric peaks related to the (001) planes of the Na_2IrO_3 phase confirming its out-of-plane preferential orientation. Two minor additional peaks with intensities below

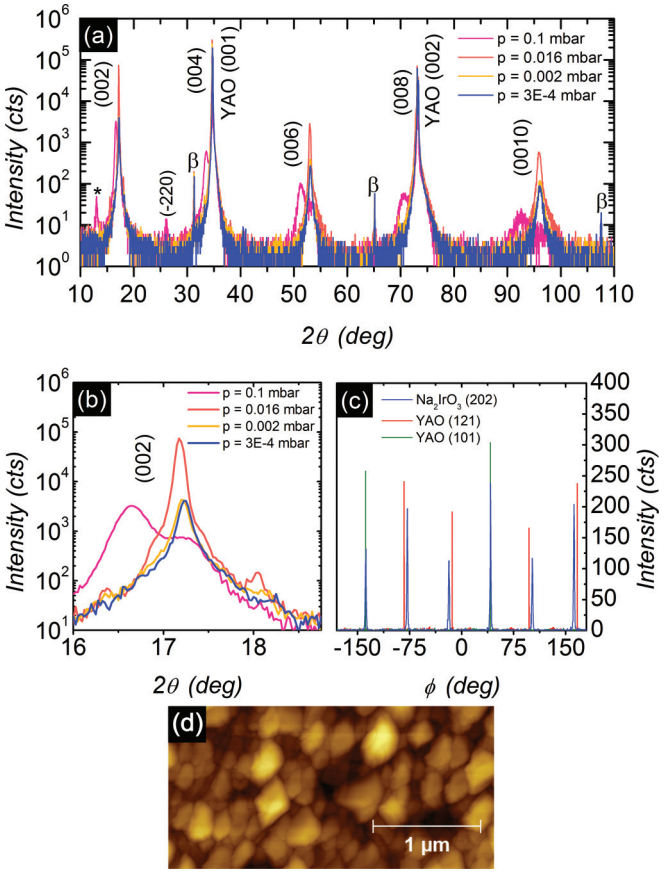

FIG. 1. (Color online) PLD-grown (001)-oriented Na_2IrO_3 films on $YAlO_3$ (001) (YAO). (a) XRD 2Θ-ω scans of films grown at p_{O2} as indicated. (b) Zoom-in on the (002) reflections seen in (a). (c) Typical XRD ϕ scans of asymmetric Na_2IrO_3 (202), YAO (101), and (121) reflections indicating the presence of six rotation domains ($p_{O2} = 3.0 \times 10^{-4}$ mbar, $T \approx 600$ °C). (d) Noncontact AFM topographic image of a typical Na_2IrO_3 film surface.

10^2 counts can be related either to the (-220) orientation of the same phase or possibly to the (110) orientation of the closely related $Na_4Ir_3O_8$ phase [denoted as $*$ in Fig. 1(a)]. Decreasing p_{O2}, we furthermore observe a clear tunability of the out-of-plane lattice parameter c from 10.813 Å to 10.435 Å as can be seen in Fig. 1(b). A variation in growth temperature and substrate material has a comparably small effect on c (see Ref. 26 and Supplemental Material). To illustrate the in-plane epitaxial relationship, Fig. 1(c) shows ϕ scans of the asymmetric Na_2IrO_3 (202) and the YAO (101) and (121) reflections. From the mismatch between rotational symmetry C_n and C_m of film and substrate, which is C_1 for Na_2IrO_3 and C_2 for YAO, one expects to observe two rotational domains,[27] i.e., two reflections in a ϕ scan of the Na_2IrO_3 (202) reflection. Instead, we observe six reflections and assume that this increased number of rotational domains is either due to a mixed terminated surface of the YAO substrate containing half unit cell step heights[28] or other nearly fulfilled additional symmetries of the substrate surface.[29] The latter can be estimated for the YAO (121) and (101) reflections, as shown in Fig. 1(c). A noncontact atomic force microscopy (AFM) scan of a thin film grown on YAO(001) is shown in Fig. 1(d). Although XRD confirms the good out-of-plane and in-plane

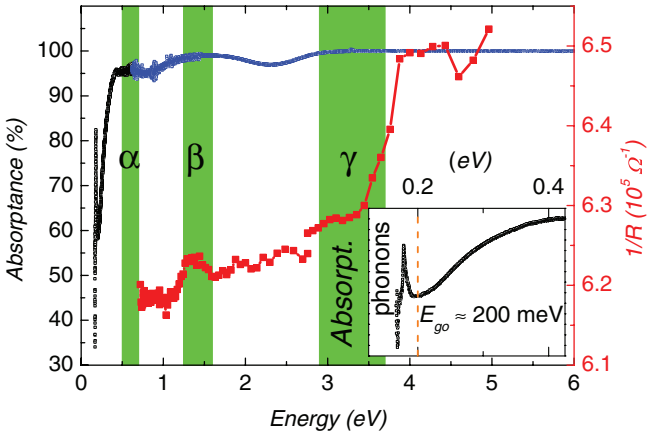

FIG. 2. (Color online) Optical absorptance measured with FTIR (black) and UV/VIS spectrometer (blue, both left scale) and optical conductivity under illumination with a Xe lamp (red, right scale) of Na_2IrO_3 thin films at ambient conditions. Full measured spectral range from 0 to 6 eV shows three absorption peaks α, β, γ at 0.6, 1.5, and above 3 eV, respectively. The inset shows the FTIR data below 0.5 eV indicating a small optical gap of $E_{go} \approx 200$ meV.

epitaxy of our films, the $1.5 \times 3\ \mu m^2$ topographic image reveals a granular surface structure with an rms roughness at the given growth conditions of 13 nm. Typical grain sizes range from 100 to 200 nm.

Figure 2 displays the results of optical measurements performed on two samples, one grown on a-sapphire, the other on c-sapphire. We employed a total of three methods to cover a total energy range of optical excitations from IR to UV, i.e., from 0.025 to 6.20 eV. Optical transmission between 0.025 and 0.992 eV is shown in black, while optical transmission data from 0.62 to 6.20 eV is shown in blue. Photoconductance G between 0.72 and 4.96 eV is shown in red. The transmission data are displayed as absorptance $(1 - T)$. In optical transmission experiments we have always measured the transmission $T_{substrate}$ of the bare substrate, as well. From the data shown in Fig. 2, we eliminated this contribution from the substrate to the signal via $T = T_{film} \times 100/T_{substrate}$. The raw data can be found in the Supplemental Material. In the FTIR data (black), we observe an absorption edge starting at $E_{go} \approx 200$ meV indicating a small optical gap compatible with the recent finding[22] of a 340 meV gap in Na_2IrO_3 single crystals. In the combination of all three data sets we observe slight indications of three absorption peaks denoted in Fig. 2 as α, β, and γ at around 0.6, 1.5, and above about 3 eV, respectively. Feature α can be discerned at the borderline of FTIR and UV/VIS data. In UV/VIS, feature β presents itself as a very broad peak from about 1.0 to 2.5 eV with a maximum at 1.5 eV. A very similar feature with much lower linewidth can be seen in the photoconductance data (red) between 1.0 and 1.7 eV with a maximum at 1.4 eV. Furthermore, photoconductance reveals the onset of excitations above 3.5 eV (feature γ). We argue that these features are indeed physical. Optical transitions with absorption peaks at very similar energies as well as small insulating gaps were previously observed in optical conductivity measurements of related materials Sr_2IrO_4[5,30] and Ir_2O_4.[31] Their crystal structure is

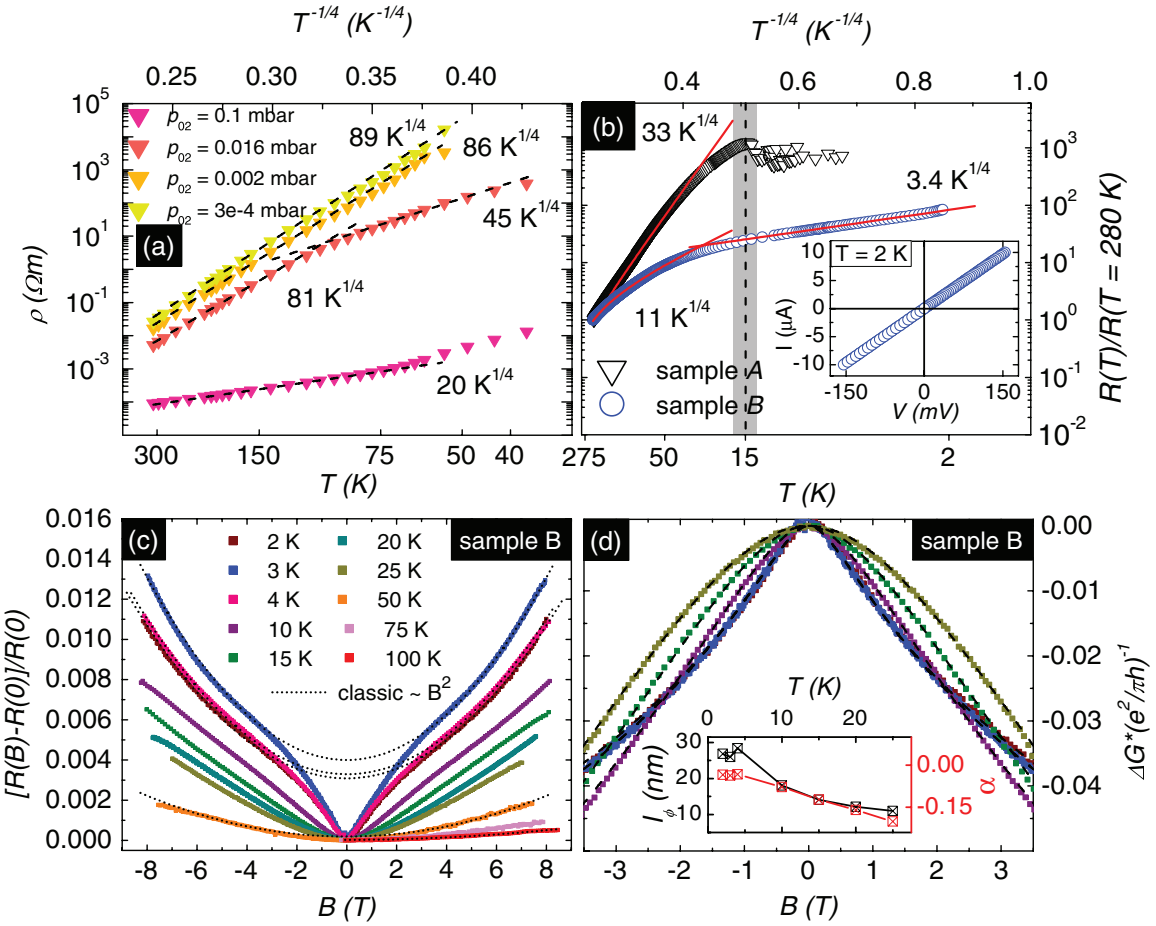

FIG. 3. (Color online) Transport properties. (a) Temperature-dependent resistivity of Na_2IrO_3 thin films grown at 550 °C on YAO(001). Data are plotted in $\log \rho$ versus $T^{-1/4}$. Straight line fits with the respective slopes $T_0^{1/4}$ indicate Mott-VRH conductivity mechanism. (b) Resistance R versus T plotted in log-log scale measured from 280 K to 2 K of two samples A, B (see text). Sample A shows an anomaly around 15 K (dashed line) related to reported antiferromagnetic ordering temperatures T_N of Na_2IrO_3 single crystals. Red lines are fits according to Mott-VRH model. Inset: Current-voltage characteristic of sample B at 2 K. (c), (d) Magnetoresistance of sample B. WAL behavior in a Na_2IrO_3 film on c-sapphire. (c) Normalized out-of-plane magnetoresistance $\Delta R/R(0)$ between 2 and 100 K. In large fields $B \geqslant 4$ T, experimental data follow a classical parabolic law (dotted lines). (d) The same data expressed as normalized magnetoconductivity $\Delta G\,(e^2/\pi h)^{-1}$ are fitted by the HLN equation for $T \leqslant 25$ K and magnetic fields $B \leqslant 3$ T (dashed lines; see text). The inset illustrates the temperature dependence of the fit parameters α and l_ϕ.

also similar consisting mainly of IrO_6 octahedra. A comparison with recent angle-resolved photoelectron spectroscopy data of Na_2IrO_3 single crystals[22] suggests that features α and β can be assigned to intraband transitions within the split Ir $5d$-t_{2g} manifold, while feature γ indicates interband transitions from Ir $5d$-t_{2g} into O $2p$ states. The splitting of the t_{2g} bands was proposed previously[22,32,33] due to an interplay between spin-orbit coupling, electronic correlations, and possible trigonal distortions of the IrO_6 octahedra. Trigonal distortions in turn are deemed necessary to facilitate the experimentally observed[19,20] zigzag type antiferromagnetic order.

Figure 3(a) shows the electrical resistivity $\log \rho$ versus $T^{-1/4}$ between 300 K and 30 K for a series of Na_2IrO_3 thin films grown on YAO(001) at $T \approx 550$ °C. For all oxygen pressures, the films show semiconducting behavior. For thin films grown at $p_{O2} = 0.1$ mbar, resistivity at 300 K is around 2.4×10^{-4} Ω m. It monotonically increases to 2.8×10^{-2} Ω m for $p_{O2} = 3 \times 10^{-4}$ mbar, thus demonstrating the tunability of resistivity (see Table I). At $p_{O2} = 0.002$ mbar and lower, resistivity exceeds our measuring range of 6 MΩ at low temperatures. The temperature dependence of resistivity between 300 and 40 K can be described using a three-dimensional Mott variable-range hopping (VRH) model,[23] for which

$$\rho = \rho_0 \exp[(T_0/T)^{1/4}]. \quad (1)$$

This is indicated by the straight line fits in Fig. 3(a). Thus, we observe VRH similarly as previously observed in single-crystalline Na_2IrO_3[11] and Sr_2IrO_4.[34] The localization temperature T_0 of the VRH model is given by[35]

$$T_0 = 21.2/k_B a^3 N(E_F), \quad (2)$$

where k_B is Boltzmann's number, a is the localization length, i.e., the decay radius of its wave function, and $N(E_F)$ is the density of states at the Fermi level.[23] VRH is usually associated with the localization of carriers by disorder. Fitting the experimental resistivity results using Eq. (1), we obtain T_0 comparable with various other transition-metal oxides[36–40]

TABLE I. Na_2IrO_3 thin films grown on YAO(001) at $T \approx 550\,^{\circ}C$ and oxygen partial pressures p_{O2}: Room temperature resistivity $\rho(T = 300\ K)$, ρ_0, and T_0 are fit parameters according to Eq. (1). a was calculated using Eq. (2) assuming $N(E_F) = 10^{28}\ eV^{-1}\,m^{-3}$.

p_{O2} (mbar)	$\rho(T = 300\ K)$ (Ω m)	ρ_0 (Ω m)	T_0 (K)	a (Å)
0.01	8.0×10^{-5}	6.5×10^{-7}	1.7×10^{5}	5.29
0.016 (300 to 125 K)	5.2×10^{-3}	1.9×10^{-11}	4.4×10^{7}	0.82
0.016 (91 to 40 K)	5.2×10^{-3}	2.9×10^{-6}	4.0×10^{6}	1.83
0.002	1.6×10^{-2}	2.0×10^{-11}	5.6×10^{7}	0.76
3×10^{-4}	2.6×10^{-2}	1.8×10^{-11}	6.3×10^{7}	0.73

(see Table I). Using Eq. (2) it is then possible to calculate a or $N(E_F)$. However, knowledge of either a or $N(E_F)$ is required. Here, we assume a constant $N(E_F)$ on the order of $10^{28}\ eV^{-1}\,m^{-3}$. We estimated $N(E_F)$ from heat capacity measurements performed on various iridates,[37,41–44] where the coefficient η was obtained from a fit of $C/T = \eta + \beta T$ at low temperatures. In these materials, the coefficient η ranges from 0.5 to 10 $mJ\,K^{-2}\,mol\text{-}Ir^{-1}$ and is related to $N(E_F)$ via $\eta = \pi^2 k_B^2 V_m N(E_F)/3$, with V_m being the molar volume of Ir. The localization lengths a calculated from the fitted T_0 and constant $N(E_F)$ using Eq. (2) are on the order of 1 Å and given in Table I. Their magnitude is reasonable in comparison with the reported Ir-Ir and Ir-O bond distances in Na_2IrO_3 of about 3 and 2 Å, respectively.[19,20] According to our calculation we observe a correlation between a and the resistivity; i.e., as a decreases we observe a dramatic increase in resistivity ρ.

Figure 3(b) shows the normalized resistance $R(T)/R(T = 280\ K)$ between 280 and 2 K of two samples A and B grown at 0.016 mbar and $T \approx 550\,^{\circ}C$ on YAO(001) and c-sapphire, respectively. R was measured by the van der Pauw and four-point methods for samples A and B, respectively. Sample B was furthermore capped by a 110 nm thick SiN_x layer and used for magnetoresistance measurements discussed in the next section. The current-voltage characteristic of sample B at 2 K, shown in the inset of Fig. 3(b), is a straight line highlighting the excellent contact quality and ohmic behavior persisting down to 2 K. Quantitative differences between the resistance curves of samples A and B most likely arise from the different substrate used. For both samples, a 3D Mott-VRH model describes the data between 280 and 50 K, however, with different slopes $T_0^{1/4} = 33\ K^{1/4}$ (A) and $T_0^{1/4} = 11\ K^{1/4}$ (B). In addition, sample A displays a sharp change in R around 15 K which can be related to the formation or suppression of scattering processes which decrease the resistance for $T <$ 15 K. A similar effect is also observed in sample B below 25 K. It is known from some antiferromagnetic (AF) materials that resistance diminishes below the Néel temperature T_N.[45–47] For single-crystalline Na_2IrO_3, literature reports on the formation of an AF phase with a Néel temperature T_N between 13.4 and 18.1 K.[11,19–21] We suggest that the decrease of the resistance below 15 and 25 K in our investigated samples A and B, respectively, is a consequence of the AF phase formation, possibly with a reduction in spin scattering. For sample B we further observe that the low-temperature resistance ($T < 25$ K) can also be well described by the Mott-VRH dependence, but with a much smaller slope of $T_0^{1/4} = 3.4\ K^{1/4}$ compared to the high-temperature range. With regard to the formation of AF long-range order and assuming the same $N(E_F)$ as before, this decrease of T_0 can be related to an increase in the electron localization length a from 12 to 56 Å. However, these values are one order of magnitude larger in contrast to the samples discussed above and suggest that a constant $N(E_F)$ for all samples is merely a simplifying assumption. As will be discussed below, we similarly observe a significant increase in the phase coherence length l_ϕ extracted from magnetoresistance for $T \leqslant 25$ K. At present, it is not understood why Mott-VRH is observed within such an extended range of temperatures in both our epitaxial films and in single crystals.[11] Theories on variable range hopping[23,35,48] require the localization of states within a narrow band near the Fermi level. In this spirit, the localization of states due to strong on-site Coulomb interactions of the Ir 5d orbitals and structural disorder induced by frequent stacking faults and interatomic site mixings[11,19] would be consistent with variable range hopping behavior. In addition, the existence of narrow Ir 5d-t_{2g} bands[22] and a small insulating gap (cf. Ref. 22 and $E_{go} \approx 200$ meV in Fig. 2) supports variable range hopping.

Out-of-plane magnetoresistance (MR) measurements performed on two samples between 2 K and 100 K are shown in Fig. 3(c). The normalized magnetoresistance $R/R(0) = [R(B) - R(0)]/R(0)$ is positive for all measured temperatures. In fields $B > 3$ T, MR scales well with B^2 which can be ascribed to the typical Lorentz contribution.[49] In fact, MR for $T \geqslant 75$ K follows this parabolic dependence for all measured fields. However, at low temperatures and at fields $B < 3$ T we observe a quick rise in MR. This behavior can be understood according to the weak antilocalization (WAL) effect. In light of recent proposals of topologically nontrivial phases present in Na_2IrO_3,[7,10,14,15] the observation of WAL is very interesting, as it has been observed in thin films of established topological insulators Bi_2Se_3[50–53] and Bi_2Te_3.[54] However, WAL is also observed in a system with strong spin-orbit coupling, such as ultrathin Sb films[55] or Mg films covered with submonolayers of Au.[56] There, WAL originates from the destructive interference of coherently backscattered conduction electrons due to spin rotations.[57] WAL is also associated with topological surface states:[58] Surface electrons acquire a Berry phase of π leading to destructive quantum interference, as well. In both cases, conductance is enhanced due to the suppression of backscattering. In a magnetoresistance experiment, the magnetic field partially destroys the destructive quantum interference and leads to an unusual rise in resistance. Experimentally, we study the observed WAL effect by fitting the low-field magnetoconductivity (MC) for $T \leqslant 25$ K shown in Fig. 3(d) with the Hikami-Larkin-Nagaoka (HLN) equation for a 2D system in the limit of strong spin-orbit

coupling:[59]

$$\Delta G(B) = -\alpha \frac{e^2}{\pi h}\left[\ln\left(\frac{\hbar}{4el_\phi^2 B}\right) - \Psi\left(\frac{\hbar}{4el_\phi^2 B}\right)\right], \quad (3)$$

where Ψ is the digamma function and l_ϕ denotes the phase coherence length. The prefactor α is expected equal to $-1/2$ for both a traditional 2D system with strong spin-orbit interactions[59] and *one* surface of a topological insulator;[50] i.e., for both the top and bottom surface of a topological insulator thin film without contribution from the bulk one expects $\alpha = -1$. Our experimental data can be fitted well by Eq. (1) for fields $B \leqslant 3$ T and $T \leqslant 25$ K as the dashed lines in Fig. 3(d) illustrate. With temperature, the cusp continuously broadens. The inset shown in Fig. 3(d) displays the temperature dependence of the extracted fit parameters α and l_ϕ. Opposed to $\alpha = -1/2$ corresponding to one surface electron channel, our fitted α decreases from -0.034 to -0.20 with increasing temperature. We also note the small values of the phase coherence length l_ϕ decreasing from 27 nm at 2 K to 11 nm at 25 K. From our fit results we infer that in our films WAL is reduced in comparison with experiments on established topological insulator thin films,[50–54] where film thickness is often below 50 nm, α ranges from -0.38 to about -1, and l_ϕ ranges from 100 nm to 1000 nm. In our films, the thickness is in the 100 nm regime, such that a dominating bulk contribution to transport properties is very likely. Deviations from $\alpha = -1/2$ can be attributed to the scattering on magnetic impurities which can lead to a reduction of WAL bringing α closer to zero.[54,59–61] Such magnetic impurities could either be inherent to the bulk or caused by contamination during sample processing. Small l_ϕ have been suggested as evidence for reduced screening and increased electron-electron interaction effects in a regime of low charge carrier densities.[50] We argue that similar detrimental effects on the phase coherence length l_ϕ can be caused by defects at the interface or increased impurity scattering due to high film thickness. It is also theorized that bulk channels with opposite effect, i.e., weak localization causing negative MR, could partially compensate the WAL of the surface channels.[62] At this point, however, a quantitative discussion on the observed WAL is merely speculative. Also, at this stage the observation of WAL is not intended as direct evidence for a topological insulator phase. First thickness-dependent transport measurements (not shown here) indicate, however, that conductivity below 40 K is nearly independent of film thickness thus hinting at a surface-dominated conduction in this range of temperatures.

We have demonstrated that heteroepitaxial Na_2IrO_3 thin films with very good out-of-plane crystalline orientation and defined in-plane epitaxial relationship can be grown by PLD on various oxide substrates. Resistivity is dominated by three-dimensional variable-range hopping. Optical experiments indicate a small optical gap $E_{go} \approx 200$ meV and a splitting of the Ir $5d$-t_{2g} manifold. For positive magnetoresistance below 3 T and 25 K we observed signatures of a weak antilocalization effect as evidence for strong spin-orbit interaction. The discovery of such an effect in Na_2IrO_3 thin films is very intriguing as it does not eliminate propositions[7,10,14,15] of a topologically nontrivial phase in this material. However, the current state of results is insufficient evidence for the existence of such a topological phase.

We thank the Deutsche Forschungsgemeinschaft (DFG) for financial support within Project No. LO790/5-1 "Oxide topological insulator thin films." J.B.Q. was supported by the Collaborative Research Center SFB 762 "Functionality of Oxide Interfaces."

*Corresponding author: marcus.jenderka@physik.uni-leipzig.de

[1] F. Wang and T. Senthil, Phys. Rev. Lett. **106**, 136402 (2011).
[2] S. Nakatsuji, Y. Machida, Y. Maeno, T. Tayama, T. Sakakibara, J. van Duijn, L. Balicas, J. N. Millican, R. T. Macaluso, and J. Y. Chan, Phys. Rev. Lett. **96**, 087204 (2006).
[3] Y. Okamoto, M. Nohara, H. Aruga-Katori, and H. Takagi, Phys. Rev. Lett. **99**, 137207 (2007).
[4] M. J. Lawler, A. Paramekanti, Y. B. Kim, and L. Balents, Phys. Rev. Lett. **101**, 197202 (2008).
[5] B. J. Kim, H. Jin, S. J. Moon, J.-Y. Kim, B.-G. Park, C. S. Leem, J. Yu, T. W. Noh, C. Kim, S.-J. Oh, J.-H. Park, V. Durairaj, G. Cao, and E. Rotenberg, Phys. Rev. Lett. **101**, 076402 (2008).
[6] B. Kim, H. Ohsumi, T. Komesu, S. Sakai, and T. Morita, Science **323**, 1329 (2009).
[7] A. Shitade, H. Katsura, J. Kuneš, X.-L. Qi, S.-C. Zhang, and N. Nagaosa, Phys. Rev. Lett. **102**, 256403 (2009).
[8] D. Pesin and L. Balents, Nat. Phys. **6**, 376 (2010).
[9] B.-J. Yang and Y. B. Kim, Phys. Rev. B **82**, 085111 (2010).
[10] C. H. Kim, H. S. Kim, H. Jeong, H. Jin, and J. Yu, Phys. Rev. Lett. **108**, 106401 (2012).
[11] Y. Singh and P. Gegenwart, Phys. Rev. B **82**, 064412 (2010).
[12] G. Jackeli and G. Khaliullin, Phys. Rev. Lett. **102**, 017205 (2009).
[13] J. Chaloupka, G. Jackeli, and G. Khaliullin, Phys. Rev. Lett. **105**, 027204 (2010).
[14] J. Wang, R. Li, S.-C. Zhang, and X.-L. Qi, Phys. Rev. Lett. **106**, 126403 (2011).
[15] H.-C. Jiang, Z.-C. Gu, X.-L. Qi, and S. Trebst, Phys. Rev. B **83**, 245104 (2011).
[16] A. Kitaev, Ann. Phys. **303**, 2 (2003).
[17] G. P. Collins, Sci. Am. **294**, 56 (2006).
[18] C. Nayak, A. Stern, M. Freedman, and S. Das Sarma, Rev. Mod. Phys. **80**, 1083 (2008).
[19] S. K. Choi, R. Coldea, A. N. Kolmogorov, T. Lancaster, I. I. Mazin, S. J. Blundell, P. G. Radaelli, Y. Singh, P. Gegenwart, K. R. Choi, S.-W. Cheong, P. J. Baker, C. Stock, and J. Taylor, Phys. Rev. Lett. **108**, 127204 (2012).
[20] F. Ye, S. Chi, H. Cao, B. C. Chakoumakos, J. A. Fernandez-Baca, R. Custelcean, T. F. Qi, O. B. Korneta, and G. Cao, Phys. Rev. B **85**, 180403 (2012).
[21] X. Liu, T. Berlijn, W.-G. Yin, W. Ku, A. Tsvelik, Y.-J. Kim, H. Gretarsson, Y. Singh, P. Gegenwart, and J. P. Hill, Phys. Rev. B **83**, 220403 (2011).

[22]R. Comin, G. Levy, B. Ludbrook, Z.-H. Zhu, C. N. Veenstra, J. A. Rosen, Y. Singh, P. Gegenwart, D. Stricker, J. N. Hancock, D. van der Marel, I. S. Elfimov, and A. Damascelli, Phys. Rev. Lett. **109**, 266406 (2012).
[23]N. F. Mott, Philos. Mag. **19**, 835 (1969).
[24]M. Lorenz, C. Schmidt, G. Benndorf, T. Böntgen, H. Hochmuth, R. Böttcher, A. Pöppl, D. Spemann, and M. Grundmann, J. Phys. D **46**, 065311 (2013).
[25]See Supplemental Material at http://link.aps.org/supplemental/10.1103/PhysRevB.88.045111 for further experimental details, XRD data of the other oxide substrates, further resistivity data, and the raw optical transmission data.
[26]M. Jenderka, master's thesis, Universität Leipzig, 2012.
[27]M. Grundmann, T. Böntgen, and M. Lorenz, Phys. Rev. Lett. **105**, 146102 (2010).
[28]J. E. Kleibeuker, G. Koster, W. Siemons, D. Dubbink, B. Kuiper, J. L. Blok, C.-H. Yang, J. Ravichandran, R. Ramesh, J. E. ten Elshof, D. H. A. Blank, and G. Rijnders, Adv. Funct. Mater. **20**, 3490 (2010).
[29]M. Grundmann, Phys. Status Solidi B **248**, 805 (2011).
[30]S. J. Moon, H. Jin, K. W. Kim, W. S. Choi, Y. S. Lee, J. Yu, G. Cao, A. Sumi, H. Funakubo, C. Bernhard, and T. W. Noh, Phys. Rev. Lett. **101**, 226402 (2008).
[31]H. Kuriyama, J. Matsuno, S. Niitaka, M. Uchida, D. Hashizume, A. Nakao, K. Sugimoto, H. Ohsumi, M. Takata, and H. Takagi, Appl. Phys. Lett. **96**, 182103 (2010).
[32]H. Jin, H. Kim, H. Jeong, C. H. Kim, and J. Yu, arXiv:0907.0743.
[33]S. Bhattacharjee, S.-S. Lee, and Y. B. Kim, New J. Phys. **14**, 073015 (2012).
[34]G. Cao, J. Bolivar, S. McCall, and J. E. Crow, Phys. Rev. B **57**, 11039(R) (1998).
[35]B. Shklovskii and A. Efros, *Moscow Izdatel Nauka* (Springer, Berlin, 1984).
[36]M. A. Kastner, R. J. Birgeneau, C. Y. Chen, Y. M. Chiang, D. R. Gabbe, H. P. Jenssen, T. Junk, C. J. Peters, P. J. Picone, T. Thio, T. R. Thurston, and H. L. Tuller, Phys. Rev. B **37**, 111 (1988).
[37]M. Bremholm, S. Dutton, P. Stephens, and R. Cava, J. Solid State Chem. **184**, 601 (2011).
[38]R. H. Colman and A. C. McLaughlin, Phys. Rev. B **85**, 144419 (2012).
[39]A. Yildiz, S. Lisesivdin, M. Kasap, and D. Mardare, J. Non-Cryst. Solids **354**, 4944 (2008).
[40]M. Lorenz, H. von Wenckstern, and M. Grundmann, Adv. Mater. **23**, 5383 (2011).
[41]J. Zhao, L. Yang, Y. Yu, F. Li, R. Yu, and C. Jin, Inorg. Chem. **48**, 4290 (2009).
[42]N. S. Kini, A. M. Strydom, H. S. Jeevan, C. Geibel, and S. Ramakrishnan, J. Phys.: Condens. Matter **18**, 8205 (2006).
[43]N. Taira, M. Wakeshima, and Y. Hinatsu, J. Phys.: Condens. Matter **13**, 5527 (2001).
[44]S. A. Carter, B. Batlogg, R. J. Cava, J. J. Krajewski, W. F. Peck, and L. W. Rupp, Phys. Rev. B **51**, 17184 (1995).
[45]A. Fote, H. Lutz, T. Mihalisin, and J. Crow, Phys. Lett. A **33**, 14 (1970).
[46]W. Jiang, J. L. Peng, J. J. Hamilton, and R. L. Greene, Phys. Rev. B **49**, 690 (1994).
[47]K.-A. Lorenzer, M. Inamdar, L. Shafeek, A. Prokofiev, and S. Paschen, J. Phys.: Conf. Ser. **391**, 012036 (2012).
[48]V. Ambegaokar, Phys. Rev. B **4**, 2612 (1971).
[49]J. Ziman, *Electrons and Phonons: The Theory of Transport Phenomena in Solids* (repr.; Clarendon Press, Oxford, 2007).
[50]J. Chen, H. J. Qin, F. Yang, J. Liu, T. Guan, F. M. Qu, G. H. Zhang, J. R. Shi, X. C. Xie, C. L. Yang, K. H. Wu, Y. Q. Li, and L. Lu, Phys. Rev. Lett. **105**, 176602 (2010).
[51]J. Chen, X. Y. He, K. H. Wu, Z. Q. Ji, L. Lu, J. R. Shi, J. H. Smet, and Y. Q. Li, Phys. Rev. B **83**, 241304 (2011).
[52]Y. S. Kim, M. Brahlek, N. Bansal, E. Edrey, G. A. Kapilevich, K. Iida, M. Tanimura, Y. Horibe, S. W. Cheong, and S. Oh, Phys. Rev. B **84**, 073109 (2011).
[53]A. A. Taskin, S. Sasaki, K. Segawa, and Y. Ando, Adv. Mater. **24**, 1 (2012).
[54]H. T. He, G. Wang, T. Zhang, I. K. Sou, G. K. L. Wong, J. N. Wang, H. Z. Lu, S. Q. Shen, and F. C. Zhang, Phys. Rev. Lett. **106**, 166805 (2011).
[55]B. Hermann and P. Haier, Phys. Status Solidi B **205**, 241 (1998).
[56]G. Bergmann, Phys. Rev. Lett. **48**, 1046 (1982).
[57]G. Bergmann, Phys. Rep. **107**, 1 (1984).
[58]L. Fu and C. L. Kane, Phys. Rev. B **76**, 045302 (2007).
[59]S. Hikami, A. Larkin, and Y. Nagaoka, Prog. Theor. Phys. **63**, 707 (1980).
[60]D. Lükermann, S. Sologub, H. Pfnür, C. Klein, M. Horn–von Hoegen, and C. Tegenkamp, Phys. Rev. B **86**, 195432 (2012).
[61]M. Liu, J. Zhang, C.-Z. Chang, Z. Zhang, X. Feng, K. Li, K. He, L.-l. Wang, X. Chen, X. Dai, Z. Fang, Q.-K. Xue, X. Ma, and Y. Wang, Phys. Rev. Lett. **108**, 036805 (2012).
[62]H.-Z. Lu and S.-Q. Shen, Phys. Rev. B **84**, 125138 (2011).